Polarimetric detection of laser induced ultrashort magnetic pulses in overdense plasma

Subhendu Kahaly,[1,a)] S. Mondal,[1] G. Ravindra Kumar,[1] S. Sengupta,[2] A. Das,[2] and P. K. Kaw[2]
[1]*Tata Institute of Fundamental Research, 1 Homi Bhabha Road, Mumbai 400005, India*
[2]*Institute for Plasma Research, Bhat, Gandhinagar 382428, India*

(Received 27 June 2008; accepted 24 March 2009; published online 22 April 2009)

The interaction of intense ($\sim 10^{16}$ W cm^{-2}), subpicosecond pulses with solid targets can generate highly directional jets of hot electrons. These electrons can propagate in the solid along with the counterpropagating return shielding currents. The spontaneous magnetic field that is generated by these currents, captures in its time evolution, important information about the dynamics of the complex transport processes. By using a two pulse pump-probe polarimetric technique the temporal evolution of multimegagauss magnetic fields is measured for optically polished BK7 glass targets, each coated with a thin layer of either copper or silver. A simple model is then used for explaining the observations and for deducing quantitative information about the transport of hot electrons.
 [DOI: 10.1063/1.3118586]

I. INTRODUCTION

The interaction of ultraintense, ultrashort laser pulses with solid density materials, leads to extreme states of matter under laboratory conditions. Such tiny and explosively ionized plasmas house the largest and shortest lived magnetic fields on Earth[1] and are important sources of coherent and incoherent electromagnetic radiation,[2] fast ions, and electrons across a wide energy range.[3]

It has been shown both theoretically and experimentally that at high intensities light is absorbed in such a short lived plasma by many collisionless mechanisms such as $j \times B$ heating (ponderomotive acceleration),[4–6] vacuum heating,[7,8] and resonance absorption[9–11] (RA) resulting in the generation of hot electron currents which are in the form of jets. These jets propagate along the direction of laser axis in case of $j \times B$ heating,[5,12] while in RA the propagation is along the direction of target normal[9–11] [see Fig. 2(a) below]. The medium, in turn, responds to the hot electron current by setting up an equivalent charge neutralizing return current[13] so that the net current is always below the *Alfvén* limit.[14–16] This resultant current generates huge pulses of azimuthal [Fig. 2(a)], quasistatic magnetic field[17] whose evolution captures the complex transport of hot electrons through the dense medium. The knowledge of such transport processes is crucial for fast ignition (FI) scheme of inertial fusion.[18,19] The success of FI, in fact, depends on the generation of hot electrons, their collimation, transport, and eventual stopping in the overdense region of the plasma. The estimation of hot electron stopping length and factors affecting it, are therefore, extremely important. Further, a recent simulation has reported the possibility of controlling of hot electron collimation by application of large magnetic fields generated by a second pulse incident at a proper time delay.[20] The dynamics of the laser generated magnetic field has thus become an important issue in itself.

The first experimental observation of spontaneous laser generated magnetic field (approximately kilogauss) in laser-solid interaction was reported by Stamper *et al.* in 1971.[21] The first optical experiment realized in 1975 by Stamper *et al.* showed that the magnetic fields were in the megagauss range.[22] Since then there have been many studies on various aspects of the magnetic field.[23–28] Various innovative techniques such as measurement of higher harmonic cutoffs[1] and proton radiography[29–31] have been applied to probe the magnetic field in the overdense region of laser generated plasma, but there have been very few reports on the temporal dynamics of the process with subpicosecond time resolution.[32–34]

In this paper we present femtosecond time resolved pump-probe polarimetry to decipher the evolution of megagauss magnetic fields generated near the critical density layer in two different types of targets. The hot electrons are generated in thin solid density plasma layers in Cu and Ag and their propagation is studied in BK7 glass medium. Section II contains a description of our experimental setup and detection technique. In Sec. III, we present our experimental observations and in Sec. IV we present a theoretical model which explains the temporal behavior of the measured MG magnetic fields. We also use this model to estimate the background conductivity under *in situ* conditions of high temperature and pressure, where equation of state may not be known exactly. Finally Sec. V contains our conclusion.

II. EXPERIMENTAL SETUP AND DETECTION TECHNIQUE

The experiments are performed using a Ti:sapphire chirped pulse amplified laser emitting 100 fs, 10 Hz pulses at 800 nm. Under optimum extraction, the prepulse (13 ns before the main pulse) intensity level is less than 10^{-6} of the main pulse. The prepulse or the pedestal do not cause significant plasma formation under our experimental

[a)]Present address: Laboratoire d'Optique Appliquée, Ecole Polytechnique, ENSTA, CNRS, UMR 7639, 91761 Palaiseau, France.

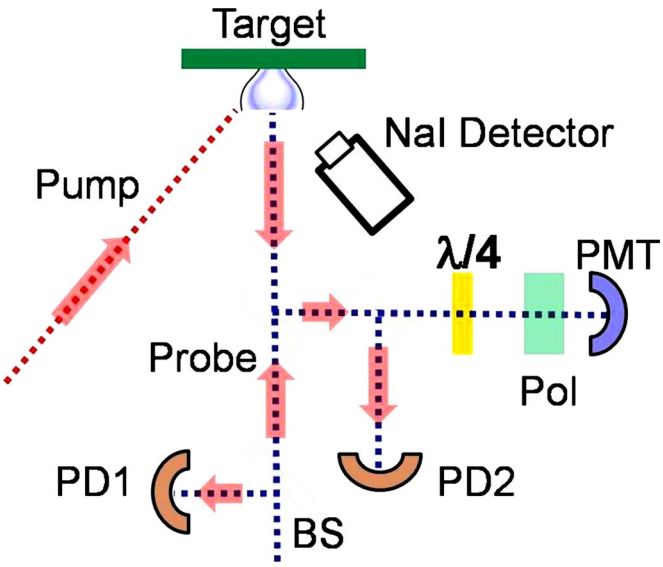

FIG. 1. (Color online) Experimental setup: beam splitter (BS), photodiodes (PD1, PD2), photomultiplier tube (PMT), quarter wave plate (λ/4), and polarizer (Pol).

conditions.[35] The schematic of the experimental setup is shown in Fig. 1. The *p* polarized laser is focused at oblique incidence (45°) with a *f*/10 lens on optically polished (roughness ~λ/5) BK7 glass targets coated with Cu or Ag metal, housed in a vacuum chamber at 10^{-3} torr. The target is constantly moved with the help of a computer controlled precision *x*-*y* stage, during the experiment so that each pulse irradiates a fresh spot. The maximum main pulse energy used in the experiments is limited to 8 mJ, giving a peak intensity of about 3.4×10^{16} W cm^2 in a 20 μm diameter focal spot. The thickness of metal coating on the BK7 glass targets is 1 μm which is $\gg\delta_s\sim c/\omega_p$, the optical skin depth at 800 nm ($\sim10^{-2}$ μm). So the incident intense ultrashort light essentially interacts with only the metallic layer with the glass background playing no direct role in the absorption of light. The metallic foreground acts as a source of hot electrons which then propagate through the glass medium. We use second harmonic (400 nm) normally incident probe beam so that it can sample the overdense regions (until four times the critical density of pump, i.e., until $4n_c$) where large hot electron densities and high magnetic fields are expected to occur [Fig. 2(b)]. The probe is a factor of 10^3–10^4 weaker than the pump and is delayed with the help of a high resolution translation stage. The spatial overlapping of the two pulses is monitored online using a charge coupled device coupled to a microscope zoom lens looking directly at the interaction volume. The temporal matching is ascertained by looking at the sharp dip in the time resolved reflectivity of the probe pulse when the pump pulse forms plasma on the metal surface. Hot electron temperature was measured by looking at the hard x-ray bremsstrahlung emission spectrum from the plasma using a thallium activated NaI scintillating detector along the plasma plume. The details of our x-ray diagnostics are described elsewhere.[35]

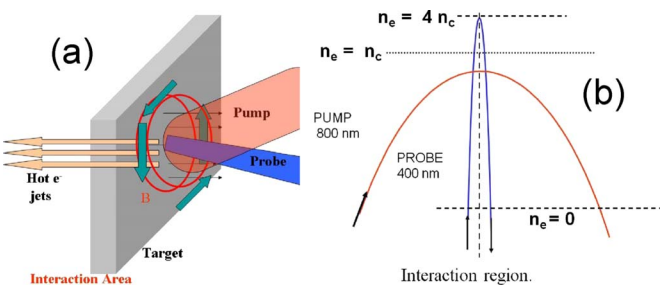

FIG. 2. (Color online) (a) Expanded view of interaction region. (b) The second harmonic probe pulse penetrates the region overdense for the pump pulse.

Under our experimental conditions the self-generated magnetic field is predominantly in the azimuthal direction because the hot electron jets penetrate normally into the target as shown in Fig. 2(a). The laser generated plasma under the effect of a magnetic field becomes birefringent and/or optically active depending on the propagation direction of the electromagnetic wave. The first is a linear anisotropy which produces the Cotton–Mouton effect (induced ellipticity) and the second is circular plasma anisotropy resulting in the Faraday effect (rotation of the polarization vector).[36] The normally incident probe wave vector **k** in our case is perpendicular to the spontaneous magnetic field **B**. A linearly polarized electromagnetic wave traveling through magnetized plasma with wave vector perpendicular to the quasistatic magnetic field acquires ellipticity due to (a) difference in refractive indices for the two characteristic modes, the ordinary mode (*O*-wave, $\mathbf{E}\|\mathbf{B}$) and the extraordinary mode (*X*-wave, $\mathbf{E}\perp\mathbf{B}$) (Refs. 36 and 37) and (b) the different turning points (cutoffs) for *O*-wave and *X*-wave. The time resolved measurement of Stokes parameters[37,38] of the reflected probe yields the magnetic field induced instantaneous ellipticity.[37]

The reflected probe is divided in two parts for simultaneous measurements of induced ellipticity as well as reflectivity. The first arm has a calibrated photodiode to measure reflectivity which is used to establish the zero of time delay and, in the other arm we use a combination of quarter wave plate and polarizer (the latter with an extinction ratio 10^{-5}) in front of a photomultiplier tube (PMT) to measure ellipticity (see Fig. 1). The four Stokes parameters are obtained by measuring light intensity with (a) only the polarizer oriented with its axis at 0°, 45°, 90°, and (b) the combination of polarizer a quarter wave plate (quarter wave plate axis at 90° and polarizer axis at 45°, where the 0° direction is arbitrary). This yields the magnetic field induced ellipticity and also rules out any presence of random depolarization in the beam.[37,38] The possible contribution to ellipticity due to refraction effects is estimated by solving Helmholtz equations and is found to be negligibly small compared to the observed magnetically induced ellipticity. Aligning the 0° direction of polarizer axis along the major axis of laser polarization vector, the ellipticity can then be simply determined by taking the ratio of transmitted intensity with polarizer at 90° and 0° for each time delay between pump and probe. Thus experimental ellipticity due to magnetic field can be obtained for any material.

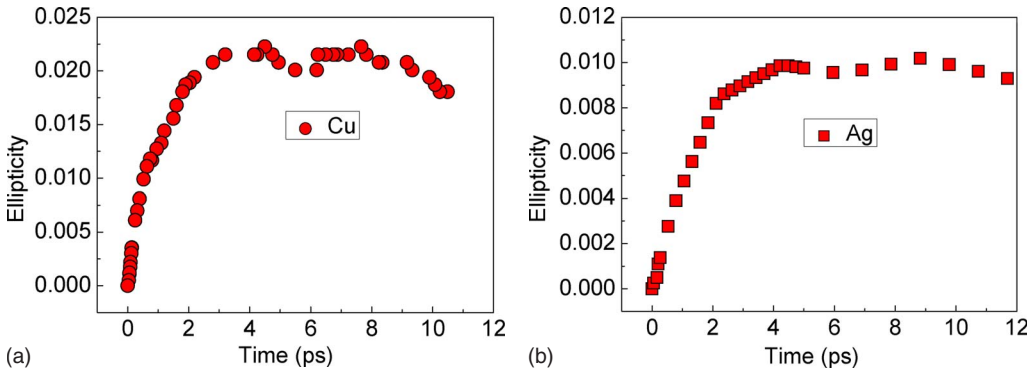

FIG. 3. (Color online) Induced ellipticity of probe as a function of delay time for Cu and Ag.

III. EXPERIMENTAL OBSERVATION

We consider two media with different atomic numbers and initial conductivities—Ag and Cu as hot electron sources in our experiment. The experimentally observed hard x-ray spectrum in each case yields similar hot electron temperatures—$T_h \simeq 35$ keV (± 2 keV). The hot electrons generated in both the cases propagate through the same medium, i.e., BK7 glass in our case. Figure 3 show the magnetically induced ellipticity as a function of the time delay between pump and probe pulses for Cu and Ag coated targets, respectively. Ellipticity is obtained in each case by measuring the Stokes parameter of probe pulse at each time delay. Calculation of magnetic field involves understanding the polarization evolution inside the magnetized medium. The evolution of Stokes vector (s) inside the magnetized plasma is determined by $ds/dz=\Omega(z)\times s(z)$. Here $\Omega=(\omega/c)(\mu_O-\mu_X)$ is proportional to difference between refractive indices μ_O and μ_X of O and X-waves, which depends on strength of the magnetic field.[37] The solution of above equation is $s(z)=Ms_{\text{input}}$, where M_{ij} is the transition matrix obeying the equation $dM_i/dz=\Omega\times M_i$, and $M_i=(M_{1i},M_{2i},M_{3i})$.[37] Final output Stokes vector and hence ellipticity is obtained by integrating this equation numerically inside the plasma by dividing it into small slabs, where within each slab, the plasma parameters are assumed to be constant. By considering self-similar expansion into vacuum the density profile is obtained as[9,39] $n_e=n_c \exp[-(z-z_c)/c_s t]$, where z_c is the position of the critical density n_c for the probe beam and $c_s=\sqrt{(ZkT_e/m_i)} \approx 3\times 10^7[(Z/A)^{1/2}(T_e/keV)^{1/2}]$ cm s^{-1} (Ref. 40) is the ion sound speed. For the background electron temperature under our experimental conditions we assumed a spatially and temporally averaged value of $T_e=100$ eV.[41–43] The average ionization state Z at a temperature of 100 eV and at the laser's critical density as given by the FLYCHK code[44] is 16.3 for Cu and 17.9 for Ag. We have found that our results are insensitive to the details of the density profile as has also been found by several other authors[33,41,45,46] for small scale length plasmas ($L/\lambda \sim 0.125$ in 10 ps; these numbers have been verified using Doppler shift measurements) and to the choice of Z and T_e [even a factor of 4 variation in Z or T_e causes minor change (<0.4 MG) in the calculated B values for both the cases of Ag and Cu]. The solution $M_{ij}(z)$, and $s(z)$ can now be determined for any infinitesimally small plasma column for a given value of magnetic field **B**. Recursively solving the equation in small steps and maintaining unitarity of M, one can find the full transition matrix for the whole plasma column. From the transition matrix, the final Stokes vector can be computed which in turn gives the ellipticity of the reflected probe. At each delay this scheme is implemented and the value of magnetic field required to generate experimentally observed ellipticity is deduced. The results of the computation of the magnetic field from observed ellipticity are shown in Figs. 4(a) and 4(b) for Cu (solid circles) and Ag (solid squares) coated glass targets, respectively. We also note here that the major contribution to ellipticity comes from the high density region around the critical density of the pump, because of (a) very strong dependence of plasma birefringence on electron density and (b) location of the hot electron source near the critical density.

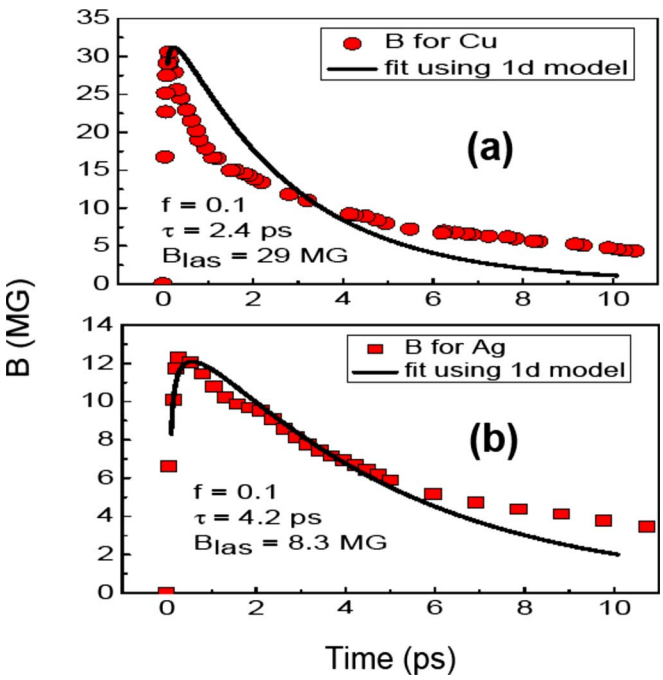

FIG. 4. (Color online) Magnetic field pulse profile for (a) Cu and (b) Ag, p polarized pump pulse.

IV. THEORETICAL MODELING AND TRANSPORT PARAMETERS

We now present a model which explains the temporal behavior of the measured magnetic fields and also allows us to estimate the background conductivities under *in situ* conditions of high temperature and pressure. The temporal evolution of magnetic field is modeled using the following equation, which describes the mechanism of quasistatic magnetic field generation under electromagnetohydrodynamic approximation:

$$\frac{\partial \vec{B}}{\partial t} = \frac{c^2}{4\pi\sigma}\nabla^2\vec{B} + \frac{c}{\sigma}(\vec{\nabla}\times\vec{j}_{\text{hot}}) + \frac{c}{en_e}(\vec{\nabla}T_e\times\vec{\nabla}n_e). \tag{1}$$

Here σ is the conductivity of the background plasma (assumed to be independent of the spatial coordinates), $\vec{j}_{\text{hot}}$ is the current density of the hot electrons, and n_e and T_e are the background electron density and temperature, respectively. We note here that in our model for magnetic field generation, we have neglected effects due to convection and plasma expansion. The justification for neglecting these effects is indicated in the later part of this section. Assuming the magnetic field to be in the azimuthal direction [Fig. 2(a)], we can use a simple one-dimensional (1D) model of hot electron propagation and Eq. (1) can be approximated as

$$\frac{\partial B}{\partial t} \approx -\frac{B_\phi}{\tau} + S(z,t), \tag{2}$$

where the diffusion term is approximated as B/τ with $\tau \approx (4\pi\sigma/c^2)(\Delta r)^2$, and the source terms are approximated as $S(z,t)\approx -[c/\sigma(\Delta r)]j_{\text{hot}}(z,t)+[c/e(\Delta r)][T_e(t)/L_s(t)]$. Here Δr is the laser spot radius which is about 10 μm and L_s is the density scale length which increases with time. There are two different temporal regimes of transport involved here: transport during the laser pulse and transport after the laser pulse (see Ref. 47) and in the experiments we see that substantial evolution of magnetic field, i.e., growth and decay takes place after the driving laser pulse is gone. The laser is on for ~100 fs and after that, the direct effects of laser radiation are not present. The laser is thus accounted for only as a source of hot electrons and modeling of magnetic field evolution becomes comparatively simpler. Taking $B=B_{\text{las}}$ at $t=\tau_{\text{laser}}$, the solution of Eq. (2) for $t>\tau_{\text{laser}}$ is given by

$$\begin{aligned} B &= B_{\text{las}}e^{-(t-\tau_{\text{laser}})/\tau} + e^{-t/\tau}\int_{\tau_{\text{laser}}}^{t} S(t,z)e^{t/\tau}dt \\ &\approx B_{\text{las}}e^{-(t-\tau_{\text{laser}})/\tau} + e^{-t/\tau}\int_{\tau_{\text{laser}}}^{t}\left(-\frac{c}{\sigma\Delta r}j_{\text{hot}}(z,t)\right. \\ &\quad \left. + \frac{c}{e\Delta r}\frac{T_e(t)}{L_s(t)}\right)e^{t/\tau}dt, \end{aligned} \tag{3}$$

where $j_{\text{hot}}=-en_hv_h$, n_h is the hot electron density, and v_h is the velocity of the hot electron fluid. We now proceed to make an estimate of the individual source terms. To make an estimate of n_h and v_h, we use the formalism given by Bell *et al.*[47] where the evolution of hot electron density (n_h) is governed by the following nonlinear diffusion equation:

$$\frac{\partial n_h}{\partial t} = \frac{\partial}{\partial z}\left(\frac{\sigma T_h}{e^2 n_h}\frac{\partial n_h}{\partial z}\right). \tag{4}$$

Here T_h is the hot electron temperature. It can be shown that the above equation is valid even without the restricted assumption of $j_{\text{total}}=j_{\text{hot}}+j_p\approx 0$, used in Refs. 47 and 48. Since our interest lies in $t>\tau_{\text{laser}}$, we use the solution of Eq. (4) in this temporal regime, as given in Ref. 47,

$$n_h = \frac{2n_0z_0}{\pi}\frac{L}{z^2+L^2}, \tag{5}$$

with

$$L(t) = z_0\left[\frac{5\pi\sigma T_h}{3e^2n_0z_0^2}(t-\tau_{\text{laser}})+1\right]^{3/5}, \tag{6}$$

where $n_0=(2/9)(I_{\text{abs}}^2\tau_{\text{laser}}e^2/\sigma T_h^3)$, $z_0=(3\sigma T_h^2/e^2I_{\text{abs}})$. The absorbed intensity $I_{\text{abs}}=fI_{\text{incident}}$, f being the fraction absorbed. The z axis is defined along the direction of plasma density gradient ∇n_e with $z=0$ corresponding to source of the hot electrons, i.e., critical density of pump beam. Here n_0 is the density of hot electrons at $z=0$, at time $t=\tau_{\text{laser}}$ and z_0 is the characteristic stopping length so that n_0z_0 represents the total number of hot electrons produced at time $t=\tau_{\text{laser}}$. The constants n_0 and z_0 have been derived by equating the absorbed laser energy $I_{\text{abs}}\tau_{\text{laser}}$ to the hot electron kinetic energy (see Ref. 47). The above solution (5) is a self-similar solution of Eq. (4) in which the shape of the spatial distribution remains the same but it expands in time with a scale length $L(t)$. Using the above expression for n_h and $L(t)$, we estimate j_{hot} as

$$j_{\text{hot}} = -en_hv_h = -e\frac{2n_0z_0}{\pi}\frac{L}{z^2+L^2}\left[\alpha\frac{dL}{dt}\right], \tag{7}$$

where v_h, the hot electron velocity is taken to be proportional to dL/dt, α being the proportionality constant. Substituting the expression for dL/dt in j_{hot} and using $\sigma \approx [c^2/4\pi(\Delta r)^2]\tau$, the first source term in the integrand of Eq. (3) becomes

$$-\frac{c}{\sigma\Delta r}j_{\text{hot}} \approx A\frac{(py\tau+1)^{1/5}e^y}{z^2+z_0^2(py\tau+1)^{6/5}}, \tag{8}$$

where $y=(t-\tau_{\text{laser}})/\tau$, $A=2cz_0\alpha T_h/e\Delta r$, and $p=5\pi\sigma T_h/3e^2n_0z_0^2$. To estimate the second source term in the integrand of Eq. (3) we use an adiabatic expansion model.[49] Assuming 1D adiabatic expansion ($\gamma=3$), we get $T_e(t)=T_e(\tau_{\text{laser}})[L_s(\tau_{\text{laser}})/L_s(t)]^2$, where $T_e(\tau_{\text{laser}})$ and $L_s(\tau_{\text{laser}})$ are, respectively, the electron temperature and density scale length at time $t=\tau_{\text{laser}}$. The temporal variation of scale length is estimated using sound speed as $dL_s/dt\approx C_s(t)\approx C_s(\tau_{\text{laser}})L_s(\tau_{\text{laser}})/L_s$, which gives

$$L_s(t) = L_s(\tau_{\text{laser}})\left(1+\frac{t-\tau_{\text{laser}}}{t_{\text{ex}}}\right)^{1/2}, \tag{9}$$

where $t_{\text{ex}}=(1/2)[L_s(\tau_{\text{laser}})/C_s(\tau_{\text{laser}})]\approx(1/2)\tau_{\text{laser}}$.

Substituting the expression for $T_e(t)$ and using Eq. (9), the second source term in the integrand of Eq. (3) becomes

TABLE I. Characteristic values.

Target	τ_{mag} (ps)	B_{max} (MG)	τ_{max} (ps)	τ (ps)	σ (s^{-1})	L_f (μm)
Cu-BK7	10	30.6	0.13	2.4	1.7×10^{14}	58
Ag-BK7	10	12.3	0.26	4.2	3.0×10^{14}	100

$$\frac{c}{e\Delta r}\frac{T_e(t)}{L_s(t)} \approx Q\left(1+\frac{y\tau}{t_{ex}}\right)^{-3/2}, \tag{10}$$

where $Q=cT_e(\tau_{laser})/[e\Delta rL_s(\tau_{laser})]$. Lastly, substituting Eqs. (8) and (10) in Eq. (3), the final expression for magnetic field stands as

$$B = B_{las}e^{-y} + Ae^{-y}\tau\int_0^y \frac{(py\tau+1)^{1/5}e^y}{z^2+z_0^2(py\tau+1)^{6/5}}dy + Qe^{-y}\tau\int_0^y\left(1+\frac{y\tau}{t_{ex}}\right)^{-3/2}e^y dy. \tag{11}$$

We use the above expression for $B(t,z)$ at $z=0$ (location of pump critical density) to model the magnetic field evolution as a function of time using τ (which is related to conductivity σ) and f as free parameters. The proportionality constant α is taken to be unity. The Beg scaling law[10] provides an estimate of hot electron temperature as $T_h \approx 100(I_{17}\lambda_{\mu m}^2)^{1/3}$ keV, where I_{17} is incident intensity in 10^{17} W cm^{-2} and $\lambda_{\mu m}$ is wavelength in μm. For the intensities used in the present set of experiments the scaling formula predicts a hot electron temperature of $T_h \sim 60$ keV. This is of the order of, but higher than the experimentally observed value ~35 keV. The background electron temperature at time $t=\tau_{laser}$ is taken to be $T_e(\tau_{laser})\approx 2$ keV (assuming 10% absorption) and $L_s(\tau_{laser})\approx C_s(\tau_{laser})\tau_{laser}$, where $C_s(\tau_{laser})$ is the sound speed estimated at $T_e \approx 2$ keV with ionization state at $t=\tau_{laser}$ as $Z=27$ (for Cu) and $Z=36$ (for Ag) as given by FLYCHK code.[44]

At time $t=\tau_{laser}$ the magnetic field, i.e., B_{las} is 29 and 8.3 MG, respectively, for copper and silver coated targets. We note here that the above magnitudes of B_{las}, have not been assumed to get a good fit with experimental data, but are actual values observed in experiments at the time $t=\tau_{laser}$. Figures 4(a) and 4(b) (solid lines) show the best fits obtained using this model. From the best fits, the relevant parameters (f being the fraction of energy absorbed by hot electrons and τ representing the magnetic field decay time) for copper and silver are—Cu: $f_{Cu}=0.1$; $\tau=2.4$ ps and Ag: $f_{Ag}=0.1$; $\tau=4.2$ ps.

From the data and the fits in Figs. 4(a) and 4(b) it is clear that the magnetic field decay time in silver glass is larger than that in copper glass. We compare the two cases to extract the conductivity parameters using $\sigma=[c^2/4\pi(\Delta r)^2]\tau$. Conductivities for two cases come out to be, $\sigma_{Cu,BK7}=1.7\times10^{14}$ s^{-1} and $\sigma_{Ag,BK7}=3\times10^{14}$ s^{-1}.

The collision frequencies inferred from the conductivities are very close to the plasma frequency at the pump critical density and are about two orders of magnitude greater than the electron-ion collision frequency obtained from Spitzer formula. This indicates that magnetic field decay is not simply due to diffusion, implying that anomalous processes too may be responsible for decay. These anomalous processes may involve both electrostatic and electromagnetic processes and also collective effects associated with return shielding currents which propagate in regions much beyond the pump critical density layer.

Using the above conductivity values and T_h from experiment, we estimate the penetration depth L_f of hot electrons [using Eq. (6)] in 10 ps as $L_{f,Cu}=5.8\times10^{-3}$ cm and $L_{f,Ag}=10.0\times10^{-3}$ cm.

Table I summarizes the characteristic parameters for the materials under study, where τ_{mag} (ps)=magnetic pulse duration, B_{max} (MG)=peak magnetic field, τ_{max} (ps)=position of peak in time, τ (ps)=decay constant, σ (s^{-1})=conductivity, and L_f (μm)=penetration in 10 ps. The measured magnetic fields around (and beyond) the critical region of the pump pulse is due to combination of forward hot electron current and the return shielding current supplied by the cold overdense plasma. As our calculation shows, the penetration depth of hot electrons $L_f \gg 1$ μm in 10 ps, clearly indicating that hot electron do penetrate significantly into BK7 glass, which gets ionized and the ionized medium in turn supplies the cold return current.

By integrating Eq. (11) with z as a variable parameter and using the values of τ and f as determined from the temporal fit above, we can obtain the magnetic field as a function of both z and t. Figures 5(a) and 5(b) shows $B(z,t)$ in the case of solid silver and copper coated glass targets, respectively, using our 1D model. In each case, as one would expect, the magnetic field diffuses in z and decays with time. Hence magnetic field pulse is not only ultrashort in time but also in localized in spatial dimension. This fact is directly related to the penetration of hot electrons into the solid conducting materials.

As stated in the beginning of this section, in our model, we have neglected effects due to convection and plasma expansion We now show that for our experimental conditions their contribution to the overall magnetic field evolution is negligible. Consider the convective term

$$|\vec{\nabla}\times(\vec{v}\times\vec{B})|. \tag{12}$$

This give rise to convection along longitudinal direction as $\sim C_sB/L$ and radial direction as $\sim C_sB/r$, where the penetration depth $L\sim 60$ μm and the spot size $r\sim 10$ μm. Using $C_s\sim 5\times10^6$ cm/s and $B\sim 30$ MG, the longitudinal convection gives ~0.03 MG/ps and the radial convection gives ~0.15 MG/ps (for Ag longitudinal and radial convection are of the order of ~0.005 and ~0.048 MG/ps, respec-

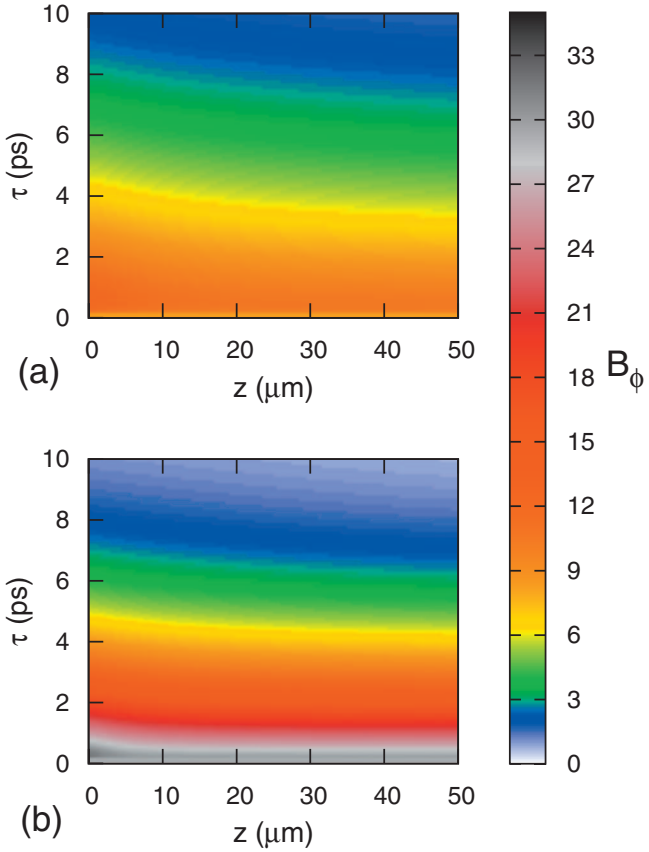

FIG. 5. (Color) The delay time (τ) and space (z) dependence of the magnetic field $B_\phi(z,\tau)$ in case of (a) Ag and (b) Cu using 1D model.

tively). We thus note that contribution due to convection and plasma expansion is negligible.

We emphasize here that the conductivities deduced above represent time and space averaged "effective conductivities" which are independent of any specific microscopic model. BK7 glass which is almost nonconducting at room temperature acquires a finite conductivity at elevated temperatures ($\sim$100 eV) due to target heating by collisional effects and ionization via large electric fields exceeding breakdown threshold.[50] These large electric fields $[\sim T_h/eL_f \sim 10$ MV/cm] are generated by the charge separation caused by the forward propagating fast electrons entering the ambient solid density plasma. This electric field not only opposes the fast electron current but also draws a return current through the cold background plasma whose magnitude, in turn, depends on the conductivity of the background. The actual dynamics of the fast electron propagation and return current generation is thus quite complex and the transport parameter (conductivity) in general has spatial and temporal dependence. To our knowledge, there does not exist any single experiment or simulation or theoretical description which completely models the above processes. Thus our measurement technique gives an order of magnitude estimate of spatiotemporal average conductivity of BK7 glass under *in situ* conditions of temperature and density.

V. CONCLUSION

In summary, we have characterized picosecond megagauss magnetic pulses generated by interaction of intense ultrashort laser pulses with solid copper and silver coated BK7 glass targets. The measurement of hot electron transport is carried out in the overdense region of the target via magnetic field profiling using second harmonic pump-probe polarimetry. Theoretical interpretation of the measured magnetic field specifically throws light on the important physical processes responsible for the magnetic field generation and further allows us to make an order of magnitude estimate of the effective conductivity of the nonconducting medium under extreme conditions where it becomes conducting. This measurement technique may have important implications for the fast ignition laser fusion scheme, where the knowledge of conductivity of the dense core is crucial for estimating the fast electron stopping length and heating of the core.[51]

ACKNOWLEDGMENTS

We thank the referee for constructive comments. G.R.K. and A.D. acknowledge their respective DAE-SRC ORI grants.

[1] M. Tatarakis, I. Watts, F. N. Beg, E. L. Clark, A. E. Dangor, A. Gopal, M. G. Haines, P. A. Norreys, U. Wagner, M. S. Wei, M. Zepf, and K. Krushelnick, Nature (London) **415**, 280 (2002).
[2] A. S. Sandhu, G. R. Kumar, S. Sengupta, A. Das, and P. K. Kaw, Phys. Rev. Lett. **95**, 025005 (2005).
[3] P. Gibbon and E. Forster, Plasma Phys. Controlled Fusion **38**, 769 (1996).
[4] S. C. Wilks, W. L. Kruer, M. Tabak, and A. B. Langdon, Phys. Rev. Lett. **69**, 1383 (1992).
[5] G. Malka and J. L. Miquel, Phys. Rev. Lett. **77**, 75 (1996).
[6] W. Yu, M. Y. Yu, J. X. Ma, Z. M. Sheng, J. Zhang, H. Daido, S. B. Liu, Z. Z. Xu, and R. X. Li, Phys. Rev. E **61**, R2220 (2000).
[7] F. Brunel, Phys. Rev. Lett. **59**, 52 (1987).
[8] M. K. Grimes, A. R. Rundquist, Y.-S. Lee, and M. C. Downer, Phys. Rev. Lett. **82**, 4010 (1999).
[9] W. L. Kruer, *The Physics of Laser Plasma Interactions* (Addison-Wesley, New York, 1988).
[10] F. N. Beg, A. R. Bell, A. E. Dangor, C. N. Danson, A. P. Fews, M. E. Glinsky, B. A. Hammel, P. Lee, P. A. Norreys, and M. Tatarakis, Phys. Plasmas **4**, 447 (1997).
[11] N. H. Ebrahim, H. A. Baldis, C. Joshi, and R. Benech, Phys. Rev. Lett. **45**, 1179 (1980).
[12] H. Teng, J. Zhang, Z. L. Chen, Y. T. Li, K. Li, X. Y. Peng, and J. X. Ma, Phys. Rev. E **67**, 026408 (2003).
[13] Y. Sentoku, K. Mima, Z. M. Sheng, P. Kaw, K. Nishihara, and K. Nishikawa, Phys. Rev. E **65**, 046408 (2002); Y. Sentoku, H. Ruhl, K. Mima, R. Kodama, K. A. Tanaka, and Y. Kishimoto, Phys. Plasmas **6**, 2855 (1999).
[14] H. Alfvén, Phys. Rev. **55**, 425 (1939).
[15] J. R. Davies, Laser Part. Beams **24**, 299 (2006).
[16] J. R. Davies, Phys. Rev. E **68**, 037501 (2003).
[17] J. A. Stamper, Laser Part. Beams **9**, 841 (1991).
[18] M. Tabak, J. Hammer, M. E. Glinsky, W. L. Kruer, S. C. Wilks, J. Woodworth, E. M. Campbell, and M. D. Perry, Phys. Plasmas **1**, 1626 (1994).
[19] R. Kodama, H. Shiraga, K. Shigemori, Y. Toyama, S. Fujioka, H. Azechi, H. Fujita, H. Habara, T. Hall, Y. Izawa, T. Jitsuno, Y. Kitagawa, K. M. Krushelnick, K. L. Lancaster, K. Mima, K. Nagai, M. Nakai, H. Nishimura, T. Norimatsu, P. A. Norreys, S. Sakabe, K. A. Tanaka, A. Youssef, M. Zepf, and T. Yamanaka, Nature (London) **418**, 933 (2002).
[20] A. P. L. Robinson, M. Sherlock, and P. Norreys, Phys. Rev. Lett. **100**, 025002 (2008).
[21] J. A. Stamper, K. Papadopoulos, R. N. Sudan, S. O. Deam, E. A. McLean, and J. M. Dawson, Phys. Rev. Lett. **26**, 1012 (1971).
[22] J. A. Stamper and B. H. Ripin, Phys. Rev. Lett. **34**, 138 (1975).

[23]M. A. Yates, D. B. van Hulsteyn, H. Rutkowski, G. Kyrala, and J. U. Brackbill, Phys. Rev. Lett. **49**, 1702 (1982).
[24]M. Borghesi, A. J. MacKinnon, A. R. Bell, R. Gaillard, and O. Willi, Phys. Rev. Lett. **81**, 112 (1998).
[25]Z. Najmudin, M. Tatarakis, A. Pukhov, E. L. Clark, R. J. Clarke, A. E. Dangor, J. Faure, V. Malka, D. Neely, M. I. K. Santala, and K. Krushelnick, Phys. Rev. Lett. **87**, 215004 (2001).
[26]P. Beiersdorfer, J. H. Scofield, and A. L. Osterheld, Phys. Rev. Lett. **90**, 235003 (2003).
[27]U. Wagner, M. Tatarakis, A. Gopal, F. N. Beg, E. L. Clark, A. E. Dangor, R. G. Evans, M. G. Haines, S. P. D. Mangles, P. A. Norreys, M.-S. Wei, M. Zepf, and K. Krushelnick, Phys. Rev. E **70**, 026401 (2004).
[28]E. Stambulchik, K. Tsigutkin, and Y. Maron, Phys. Rev. Lett. **98**, 225001 (2007).
[29]P. M. Nilson, L. Willingale, M. C. Kaluza, C. Kamperidis, S. Minardi, M. S. Wei, P. Fernandes, M. Notley, S. Bandyopadhyay, M. Sherlock, R. J. Kingham, M. Tatarakis, Z. Najmudin, W. Rozmus, R. G. Evans, M. G. Haines, A. E. Dangor, and K. Krushelnick, Phys. Rev. Lett. **97**, 255001 (2006).
[30]C. K. Li, F. H. Seguin, J. A. Frenje, J. R. Rygg, R. D. Petrasso, R. P. J. Town, P. A. Amendt, S. P. Hatchett, O. L. Landen, A. J. Mackinnon, P. K. Patel, M. Tabak, J. P. Knauer, T. C. Sangster, and V. A. Smalyuk, Phys. Rev. Lett. **99**, 015001 (2007).
[31]C. K. Li, F. H. Seguin, J. A. Frenje, J. R. Rygg, R. D. Petrasso, R. P. J. Town, O. L. Landen, J. P. Knauer, and V. A. Smalyuk, Phys. Rev. Lett. **99**, 055001 (2007).
[32]A. S. Sandhu, A. K. Dharmadhikari, P. P. Rajeev, G. Ravindra Kumar, S. Sengupta, A. Das, and P. K. Kaw, Phys. Rev. Lett. **89**, 225002 (2002).
[33]A. S. Sandhu, G. Ravindra Kumar, S. Sengupta, A. Das, and P. K. Kaw, Phys. Rev. E **73**, 036409 (2006).
[34]A. S. Sandhu, "Ultrashort–high intensity laser matter interaction studies," Ph.D. thesis, Mumbai University, 2004.
[35]P. P. Rajeev and G. Ravindra Kumar, Opt. Commun. **222**, 9 (2003).
[36]I. H. Hutchinson, *Principles of Plasma Diagnostics* (Cambridge University Press, Cambridge, 1987).
[37]S. E. Segre, Plasma Phys. Controlled Fusion **41**, R57 (1999).
[38]E. Collet, *Polarized Light* (Dekker, New York, 1993).
[39]P. Mora, Phys. Rev. Lett. **90**, 185002 (2003).
[40]S. Eliezer, *The Interaction of High-Power Lasers with Plasmas* (Institute of Physics, Bristol, 2002).
[41]H. M. Milchberg and R. R. Freeman, J. Opt. Soc. Am. B **6**, 1351 (1989).
[42]D. F. Price, R. M. More, R. S. Walling, G. Guethlein, R. L. Shepherd, R. E. Stewart, and W. E. White, Phys. Rev. Lett. **75**, 252 (1995).
[43]K. Eidmann, J. Meyer-ter-Vehn, T. Schlegel, and S. Hüller, Phys. Rev. E **62**, 1202 (2000).
[44]See http://nlte.nist.gov/FLY/. This is a website maintained by National Institute of Standards and Technology (NIST) for the code FLYCHK which generates atomic level populations and charge state distributions for a range of elements under NLTE conditions.
[45]H. M. Milchberg, R. R. Freeman, S. C. Davey, and R. M. More, Phys. Rev. Lett. **61**, 2364 (1988).
[46]M. K. Grimes, A. R. Rundquist, Y.-S. Lee, and M. C. Downer, Phys. Rev. Lett. **82**, 4010 (1999).
[47]A. R. Bell, J. R. Davies, S. Guerin, and H. Ruhl, Plasma Phys. Controlled Fusion **39**, 653 (1997).
[48]A. R. Bell, J. R. Davies, and S. M. Guerin, Phys. Rev. E **58**, 2471 (1998).
[49]J. R. Davies, personal communication (November 15, 2004).
[50]J. R. Davies, A. R. Bell, and M. Tatarakis, Phys. Rev. E **59**, 6032 (1999).
[51]J. R. Davies, Phys. Rev. E **68**, 056404 (2003).